Electron Localization and Radiation Chemistry of Amides

ARTICLE *in* THE JOURNAL OF PHYSICAL CHEMISTRY A · FEBRUARY 2012

Impact Factor: 2.69 · DOI: 10.1021/jp2115687 · Source: PubMed

2 AUTHORS:

Ilya Shkrob
Argonne National Laboratory
142 PUBLICATIONS **2,154** CITATIONS
SEE PROFILE

Timothy W Marin
Benedictine University
54 PUBLICATIONS **805** CITATIONS
SEE PROFILE

THE JOURNAL OF PHYSICAL CHEMISTRY A

Article

pubs.acs.org/JPCA

Electron Localization and Radiation Chemistry of Amides

Ilya A. Shkrob*,† and Timothy W. Marin†,‡

†Chemical Sciences and Engineering Division, Argonne National Laboratory, 9700 South Cass Avenue, Argonne, Illinois 60439, United States

‡Chemistry Department, Benedictine University, 5700 College Road, Lisle, Illinois 60532, United States

Supporting Information

ABSTRACT: Alkylamides (such as *N,N′*-dimethylformamide, *N,N′*-diethylformamide, and *N,N′*-dimethylacetamide) are aprotic solvents that are widely used in organic synthesis. These polar molecules have no electron affinity, and it is believed that irradiated liquid and solid amides stabilize excess electrons as cavity-type species analogous to hydrated and ammoniated electrons. In this study, we use isotope substitution and EPR spectroscopy to demonstrate that, in frozen amides, the suspected "cavity electron" is, in fact, a solvent-stabilized monomer anion. Our observations call into question other attributions of such features in the literature, both in low temperature solids and room temperature liquids. We also provide a general scheme describing amide radiolysis, as the related amides are used as metal ion extracting agents in nuclear separations.

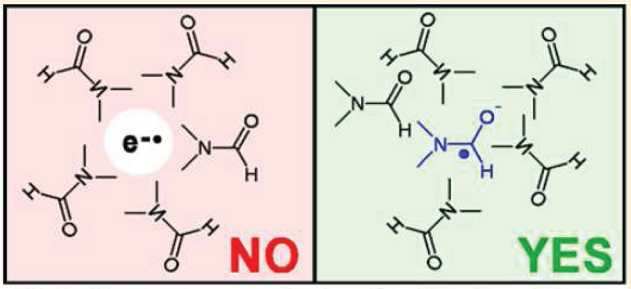

How does an excess electron localize in amides?

1. INTRODUCTION

N,N,N′,N′-Tetraalkyl substituted diamides of malonic and diglycolic acids serve as extracting agents for trivalent ions (such as lanthanides and minor actinides) in processing of spent nuclear fuel.[1] This application raises concerns about the stability of such compounds in the radiation field generated by decaying radionuclides.[1,2] In this study, we focus on the radiation chemistry of amides using monoamides as model systems. Apart from this practical interest, such systems present grounds for discussion regarding the ongoing debate on the nature of electron localization in polar media.[3−11]

The interaction of ionizing radiation with matter results in excitation and ionization of molecules (that is, the generation of excess electrons detached from their parent molecules and ejected into the solvent bulk, and "holes", i.e., the residual radical cations). These species can be localized over one or several solvent molecules or trapped in voids between the molecules.[3] The subsequent chemistry is initiated by reactions of such electrons, holes, and excited states.

In the present study, we examine the radiation chemistry of *N,N′*-dimethylformamide (DMF) and, to a lesser extent, *N,N′*-diethylformamide (DEF) and *N,N′*-dimethylacetamide (DMAc). Despite their extensive use as polar solvents in organic synthesis, the radiation chemistry of these amides has received surprisingly little attention: these solvents have not been systematically studied since the mid-1970s. The only significant development post-1980 was observation of short-lived "electrons" in neat $R_2NC(O)R'$ monoamides (where R is a methyl or ethyl group and R′ is a −H or C_1−C_3 alkyl group), *N,N,N′,N′*-tetraethylurea ($(Me_2N)_2CO$), and hexamethylphosphoramide ($(Me_2N)_3PO$, HMPA)[12−15] using nanosecond pulse radiolysis−transient absorbance spectroscopy.[15] After ionization, liquid solvents exhibited a broad, featureless absorption band centered at 0.55−0.74 eV typical of cavity-type electrons, in which the electron density is localized in a void between polarized solvent molecules. In this species, a 1s electron is stabilized by electrostatic interactions with the (induced) dipoles in several solvent molecules forming the solvation shell around the centroid of the excess electron density.[3−5] The same absorption bands are observed by dissolution of Na^0 in certain amides (e.g., HMPA).[13−15] Originally, it was hoped that the structure of solvated electrons in such aprotic liquids could be studied using electron paramagnetic resonance (EPR), given that the solvent molecules contain magnetic nuclei (^1H, ^{14}N, and ^{31}P) that couple to the unpaired electron via hyperfine interactions.[12,15−17] However, it was rapidly realized that the species initially attributed to the "solvated electron" in Na^0/HMPA were, in fact, modified Na^0 atoms.[18a] Attempts to observe trapped-electron centers in irradiated frozen neat HMPA resulted in observation of the $^{\bullet}H_2CN(Me)P(O)(NMe_2)_2$ and $(Me_2N)_2P^{\bullet}O$ radicals.[18b] The former radical is the product of hole deprotonation, while the $(Me_2N)_2P^{\bullet}O$ radical is the product of dissociative electron attachment (DEA) involving a "dry" (that is, not fully localized) electron, reaction 1:

$$(Me_2N)_3PO + e^{-\bullet} \rightarrow (Me_2N)_2P^{\bullet}O + Me_2N^- \qquad (1)$$

Received: December 1, 2011
Revised: January 20, 2012
Published: January 24, 2012

   dx.doi.org/10.1021/jp2115687 | *J. Phys. Chem. A* 2012, 116, 1746−1757

Similar reactions are known to occur for mono-, di-, and trialkyl phosphates,[19] e.g.,

$$(RO)_3PO + e^{-\bullet} \rightarrow (RO)_2P^{\bullet}O + RO^{-} \quad (2)$$

and analogous reactions were suggested for other amides, e.g.,[20]

$$R_2NC(O)R' + e^{-\bullet} \rightarrow R_2N^{-} + R'C^{\bullet}O \quad (3a)$$

$$R_2NC(O)R' + e^{-\bullet} \rightarrow R_2N^{\bullet} + R'CO^{-} \quad (3b)$$

Our estimates (Table S1 in the Supporting Information) indicate that in the gas phase reactions 3a and 3b for DMF are endergonic by 2.89 and 2.68 eV, respectively, suggesting that such reactions could only involve *prethermalized* electrons.

For *N*,*N*′-dialkylformamides (**1** in Scheme 1), the parent radical cation $\{R_2NCHO\}^{+\bullet}$ can be observed at low temperature

Scheme 1. Sketch of the Radiation Chemistry of Amides

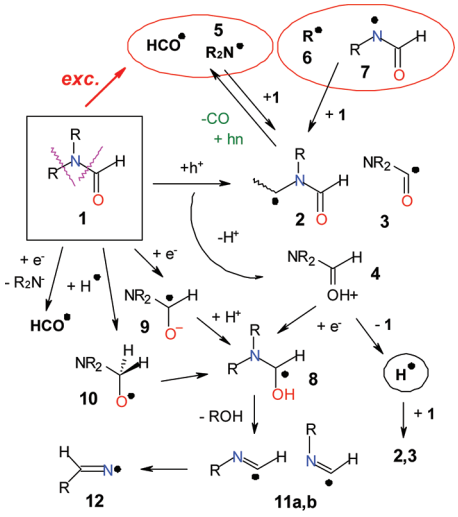

in a freon matrix.[21,22] As the sample temperature increases, this radical cation deprotonates (mainly) from the H_α position of the aliphatic arms, forming radical **2** and proton adduct **4**; this deprotonation can also occur internally, by light-induced isomerization of the parent radical cation.[21]

$$\{Me_2NC(O)H\}^{**} \rightarrow \{Me_2NCHO\}^{+\bullet} + e^{-\bullet} \quad (4)$$

$$\{Me_2NCHO\}^{+\bullet} \rightarrow {}^{\bullet}CH_2(Me)NCH(=OH^{+}) \quad (5)$$

$$\{Me_2NCHO\}^{+\bullet} + Me_2NCHO \rightarrow {}^{\bullet}CH_2(Me)NCHO + Me_2NCH(=OH^{+}) \quad (6)$$

In the gas phase (Table S1 in the Supporting Information), reaction 5 is exergonic by 0.58 eV and reaction 6 is exergonic by 0.73 eV; other modes for fragmentation (Table S1 in the Supporting Information) are endergonic, and so can only involve electronically excited "holes" formed in the course of ionization. The isomerizations in which the oxygen and nitrogen atoms serve as internal proton acceptors are endergonic by 0.37 and 0.19 eV, respectively.

For *N*,*N*,*N*′,*N*′-tetramethylurea, the corresponding radical cation decomposes to $MeNCO^{+}$ and radical **5**;[22] for DMF, the latter species can be generated by photoexcitation of radical **2** by ultraviolet (UV) light.[23] Homolytic N−C and C−H bond scission also occurs in UV excitation of the molecule in the gas phase.[24] Decarbonylation is the lowest energy channel (~0.65 eV), followed by methyl and formyl eliminations (3.5−4 eV; see also Table S1 in the Supporting Information).

In radiolysis of frozen solutions of DMF, no methyl radical, Me-loss radical **7**, or radical **5** were observed by EPR spectroscopy, despite the fact that dimethylamine was identified as a major radiolytic product (other common products being H_2, CO, and methane).[20,25] EPR studies also suggested that radicals **3** and **6** were not generated in radiolysis of DMF,[23,26] while $H_2NCO^{\bullet}$ was observed in radiolysis of formamide.[27] This is surprising, as cross recombination products traced to radical **3** were observed in product analyses.[25]

Small- and medium-size anion clusters of MeNHCHO and Me_2NCHO have not been observed in the gas phase;[28] i.e., the ability to localize electrons is restricted to large molecular aggregates. In irradiated formamide, H_2NCHO, there is only one radical attributed to reductive chemistry, viz., $H_2CN^{\bullet}$ (radical **12** in Scheme 1). Symons et al.[27] suggested that the electron fleetingly attaches to the parent molecule, forming monomer radical anion **9** (reaction 7), and subsequently eliminates hydroxide (reaction 8), yielding radical **11**, which rearranges to radical **12** (reaction 9):

$$H_2NCHO + e^{-\bullet} \rightarrow H_2NC^{\bullet}HO^{-} \quad (7)$$

$$H_2NC^{\bullet}HO^{-} \rightarrow HN{=}C^{\bullet}H + HO^{-} \quad (8)$$

$$HN{=}C^{\bullet}H \rightarrow H_2C{=}N^{\bullet} \quad (9)$$

In irradiated low-temperature DMF, there is (i) an optical absorption band[23] in the visible and near-infrared which is similar to the short-lived absorption band observed in radiolysis of liquid DMF at 300 K and attributed to the solvated electron[29] and (ii) an unresolved singlet line in the EPR spectra.[23] At 77 K, both of these features can be bleached by visible light and disappear simultaneously, suggesting a common radical progenitor.[23] In the blue, the tail of this absorption band overlaps with the band of radical **2** centered at 365 nm.[29] The "solvated electron" band in the visible disappears in the presence of electron scavengers, such as N_2O and O_2, suggesting that the progenitor is a weak electron trap.[29]

As we[6,7] and others[8,17] have stressed, solvent-stabilized (multimer) anions could be more realistic conceptual models for electron solvation than "particle-in-a-box" cavity models. There have been earlier precedents of such solvent-stabilized ions (e.g., the excess electron in acetonitrile)[30−33] that were mistaken for the "solvated electrons", and recent calculations shed doubt on whether the standard cavity model fully applies even to liquid water[4,7] and ammonia.[16,17] In sections 4 and 5, we argue that the "electron" in amides is, actually, a solvent-stabilized monomer anion (radical **9**). It has been already suspected that a radical anion of *N*-methylacetamide occurs in tetrahydrofuran[34] (a solvent which supports solvated electrons, albeit of a different type than the classical cavity electron)[35] and a radical anion of acetamide occurs in low-temperature alkaline glasses.[36,37] In tetrahydrofuran, the resulting species has a broad absorption band at 1.2 μm that stretches down to the visible region.[34] However, such observations do not exclude a cavity-type electron that is trapped by clusters of solute molecules in a less polar solvent,[38] and there is no reason to believe that electron localization in neat amide liquids occurs in the same fashion as in dilute solutions of these amides.

Below, we demonstrate that, in neat DMF, DEF, and DMAc, the unpaired electron density of the excess electron is confined to a single solvent molecule.

dx.doi.org/10.1021/jp2115687 | J. Phys. Chem. A 2012, 116, 1746−1757

To conserve space, some tables and figures have been placed in the Supporting Information. Such figures have designator "S" (e.g., Figure S1).

2. EXPERIMENTAL AND COMPUTATIONAL METHODS

Six isotopomers of *N*,*N*′-dimethylformamide (DMF) have been used in this study, abbreviated as h_7 ($(^{12}CH_3)_2{}^{14}N^{12}CHO$), d_7 ($(^{12}CD_3)_2{}^{14}N^{12}CDO$), d_6 ($(^{12}CD_3)_2{}^{14}N^{12}CHO$), d_1 ($(^{12}CH_3)_2{}^{14}N^{12}CDO$), ^{15}N ($(^{12}CH_3)_2{}^{15}N^{12}CHO$), and ^{13}CO ($(^{12}CH_3)_2{}^{14}N^{13}CHO$). Four isotopomers of *N*,*N*′-dimethylacetamide (DMAc) were used, abbreviated as h_9 ($(^{12}CH_3)_2{}^{14}N^{12}C(O)^{12}CH_3$), d_6 ($(^{12}CD_3)_2{}^{14}N^{12}C(O)^{12}CH_3$), and d_3 ($(^{12}CH_3)_2{}^{14}N^{12}C(O)^{12}CD_3$).

All of the reagents were obtained from Aldrich except for deuterated DMAc isotopomers and DMF-d_6 that were obtained from C/D/N Isotopes, Inc. The chemicals were used as supplied; as suggested by ^{1}H nuclear magnetic resonance (NMR) measurements, the DMF samples contained <1−3 mol % water.

Liquid samples were frozen by immersion in liquid nitrogen and irradiated to 3 kGy (1 Gy = 1 J/kg) at 77 K using 3 MeV electrons. The radicals were observed using a 9.44 GHz Bruker ESP300E spectrometer equipped with a flow He cryostat (Oxford Instruments CF935). The magnetic field and the hyperfine coupling constants (hfcc) are given in units of gauss (1 G = 10^{-4} T). If not stated otherwise, the first-derivative EPR spectra were obtained at 50 K using 2 G modulation at 100 kHz. The radiation-induced EPR signal from the E'_γ center in the Suprasil sample tubes was deleted from the EPR spectra. The lines from H$^\bullet$ atoms in the sample tubes were also deleted from these EPR spectra.

To examine radicals generated by oxidation of the amides, aqueous (<1 M, pH 1.9) solutions were mixed with a solution of 2 nm anatase (TiO_2) nanoparticles.[39] These colloidal solutions were flash frozen and irradiated using 500 × 40 mJ, 6 ns pulses of 355 nm light from a Nd:YAG laser. Such EPR spectra exhibit a narrow line at $g \approx 1.97$ from lattice-trapped electrons in the interior and a broad line at $g \approx 1.93$ from surface-trapped electrons ($Ti^{3+\bullet}$ ions). These interfering signals are not shown in the EPR spectra presented below (cf. Figure 1). We also carried out photochemical experiments in which amides were UV illuminated at 77 K using 200−300 nm output of a 300 W Xe arc lamp. For photobleaching experiments, we used a 60 W Xe arc lamp (>300 nm) and filtered light using a 400−900 nm band-pass filter combined with a 540 or 640 nm cutoff filter. In the following, these filter combinations are referred to as "yellow" and "red" bleaching light.

The calculations of the hfc tensors ***A*** and the optimized structures for the radicals were carried out using a density functional theory (DFT) method with the B3LYP functional[40] and 6-31+G(d,p) basis set[41] from Gaussian 98.[42] In the following, *a* denotes the isotropic hfcc and $\boldsymbol{B}_{\nu\nu}$ (ν = a,b,c) denotes the principal values of ***B*** (anisotropic part of the hfc tensor ***A***) along the principal axes. Simulations of the EPR spectra involved angular averaging of fixed-tensor radicals using first-order perturbation theory. For some of the radicals with large hfcc's, second-order effects were taken into account.

Table S2 (Supporting Information) compares the measured and calculated ionization potentials and electron and proton affinities for gas-phase DMF, the formyl radical, and the $Me_2N^\bullet$ radical (radicals **4** and **5** in Scheme 1). This comparison suggests that DFT yields reliable estimates for most of the calculated parameters; there is also good correspondence between

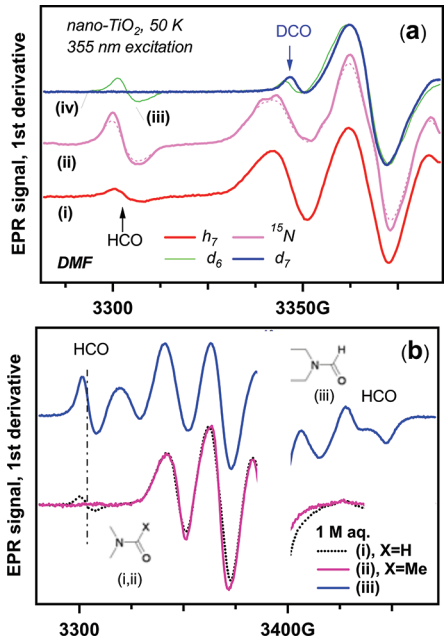

Figure 1. First-derivative EPR spectrum (9.4 GHz, 100 kHz modulation, 0.02 mW) of frozen aqueous solutions containing 1 M amides and nanoparticles of TiO_2. These solutions were irradiated by 355 nm laser light at 77 K. The EPR spectra are obtained at 50 K using a field modulation of 2 G. In panel a, EPR spectra from four isotopomers of DMF are shown: (i) h_7, (ii) ^{15}N, (iii) d_6, and (iv) d_7. The arrows indicate the low-field lines from the formyl radical, HC$^\bullet$O. The signals from trapped electron centers on TiO_2 are not shown. The dashed line in trace ii shows the EPR spectrum obtained at 2 mW. Panel b compares the EPR spectra obtained for 1 M solutions of (i) DMF-h_7, (ii) DMAc-h_9, and (iii) DEF. The vertical lines indicate the resonance lines from the formyl radical.

the calculated and experimental hfcc's for most of the radicals involved (Table S3, Supporting Information). We remind that the deuteron (spin-1) hfcc is 15.3% that of the proton (spin-1/2), and nitrogen-15 (spin-1/2) has a hfcc which is 1.43× greater than that for nitrogen-14 (spin-1). These properties, in combination with isotope substitution, can be used for analysis of overlapping signals from different radicals (see Figures S1−S3, Supporting Information). For some of these radicals (e.g., radical **5**), the rotation of pendant groups is hindered in the solid matrix, and the simulation of the EPR spectra involved averaging over random orientations of these groups (Figure S4, Supporting Information).

3. RESULTS

Before turning to radiolysis of amides, we briefly examine the radicals generated in photoexcitation (as the same excitation can occur in radiolysis) and photooxidation of amides (as the same oxidation also occurs in radiolysis). Good knowledge of spectral patterns of these radicals is prerequisite for analysis of the congested EPR spectra obtained in radiolysis.

3.1. UV Photolysis of Neat Amides. When neat DMF-h_7 or its aqueous solutions are photoirradiated by UV light at 77 K, the corresponding EPR spectra are dominated by a set of nine lines (a nonet) from radical **5** (Figure S5, Supporting Information, filled squares), with resonance lines of other radicals superimposed upon them. Due to spectral congestion, only methyl radical **6** can be identified with confidence. The comparison with the simulated EPR spectra for the $Me_2N^\bullet$

dx.doi.org/10.1021/jp2115687 | J. Phys. Chem. A 2012, 116, 1746−1757

radical (see Figures S4, S5, and S6(a), Supporting Information) indicates that the rotation of methyl groups in the dimethylamidogen radical is arrested in this DMF matrix, and the observed EPR spectrum corresponds to an ensemble of motion-frozen rotamers.

The identity of the progenitor of this nonet as radical **5** is supported by ^{15}N and d_7 substitution in DMF, as shown in Figures S4 and S6 (Supporting Information). The EPR spectrum from UV-irradiated DMF-d_7 (Figure S6(b), Supporting Information) reveals the low-field line of the DC$^{\bullet}$O radical (cf. Figure S3, Supporting Information) and the presence of another species with hfcc's corresponding to an alkyl radical, probably the $^{\bullet}CD_3$ radical.

These Observations Suggest That Homolytic N−C Bond Scission Is the Main Reaction of Photoexcited Amides in This Low-Temperature Matrix. The EPR spectra shown in Figure S7 (Supporting Information) reveal the resonance lines of $Et_2N^{\bullet}$ (for DEF) and the nonet from the $Me_2N^{\bullet}$ radical identical to the one observed in DMF-h_7 (for DMAc-h_9), respectively; in addition, there is a narrow resonance line from the acetyl radical (MeC$^{\bullet}$O) for DMAc. These observations indicate a general pattern for all amides. Interestingly, in all cases examined, N−C bond dissociation is preferred to Me−N scission with the formation of radical **7** (which has a characteristic EPR pattern, as simulated in Figure S8(a), Supporting Information).

3.2. Photoredox Reactions on Aqueous Anatase. To examine photoredox reactions of amides, we irradiated their aqueous solutions in the presence of TiO_2 nanoparticles at 355 nm. At this excitation wavelength, no direct photolysis of the amides occurs, and radicals are produced via interfacial electron transfer involving the molecules adsorbed on the surface of TiO_2; mainly the amides are oxidized by holes generated via photoinduced charge separation in this semiconducting oxide. As shown in Figure 1a (see also Figure S9, Supporting Information), the prevalent EPR signal is a triplet of resonance lines that is nearly identical for the h_7, d_1, and ^{15}N isotopomers of DMF; this triplet collapses to a singlet resonance line for the DMF-d_6 and DMF-d_7 isotopomers. Comparison to simulated EPR spectra given in Figures S1 and S2 (Supporting Information) indicates that this triplet arises from the isotopomers of radical **2**, $^{\bullet}CH_2N(Me)CHO$, as it has prominent hfcc's only in the methylene α-protons. In addition to this triplet, there is also a low-field line from the formyl radical (HC$^{\bullet}$O) observed for the DMF-h_7, DMF-d_6, and DMF-^{15}N isotopomers but is absent for the DMF-d_1 and DMF-d_7 isotopomers (Figures 1a and S9, Supporting Information). For DMF-d_7, there is a side line whose position corresponds exactly to the low-field line of the deuteroformyl (DC$^{\bullet}$O) radical.

As shown in Figure S3 (Supporting Information), **2**-h_6, **3** (regardless of the H/D substitution, as the hfcc's for the protons in this radical are negligible, see Table S3, Supporting Information), and the DC$^{\bullet}$O radical all have very similar EPR spectra. Isotope substitution (section 2) provides a means to separate their respective contributions, as the d_7-substitution collapses the triplet of lines from **2**-h_6 to a singlet resonance line from **2**-d_6 and transforms HC$^{\bullet}$O to DC$^{\bullet}$O, but it does not change the EPR spectrum of radical **3**. Thus, the side line that was observed only for DMF-d_6 (indicated with an arrow in Figure S9(a), Supporting Information) can originate only from the low-field line of radical **3**-d_6, whereas, for the DMF-d_7, both this radical and the DC$^{\bullet}$O contribute to this EPR line, which explains its slightly different shape for the DMF-d_7 and DMF-d_6 isotopomers, as shown in Figure 1a.

*These Results Suggest That Photooxidation of DMF Yields Mainly Radical **2** with Radical **3** as a Minor Side Product.* As indicated in Table S1, the energies of the C−H bonds in DMF are comparable for radicals **2** and **3** (4.19 vs 4.29 eV, respectively). Consequently, the overwhelming preference for radical **2** over radical **3** cannot be explained by these energetics alone. This preference strongly suggests that these radicals originate through deprotonation of the parent radical cation, as this reaction typically occurs from the site of maximum spin density in the radical cation; in this case, it is the methyl group of the DMF.

The identity of these radicals is further confirmed by ^{13}C substitution in the carbonyl group of the DMF (Figure S9(b), Supporting Information). Since the isotropic hfcc's for ^1H and ^{13}C in the formyl radical are comparable (Table S3, Supporting Information), this ^{13}C substitution transforms the doublet of $H^{12}C^{\bullet}O$ into a triplet from $H^{13}C^{\bullet}O$ (Figure S3, Supporting Information). The outer lines of this triplet are observed in the EPR spectra of photooxidized DMF-^{13}CO, while the triplet of lines from radical **2**-^{13}CO does not change (as the unpaired electron in this radical is weakly coupled to the carbonyl carbon). Since the formyl radical can only be the product of photoreduction, we suggest that it is generated in reaction 10 (cf. reaction 3a), which involves the trapped-electron center on TiO_2,

$$e^{-\bullet}(TiO_2) + R_2NCHO + H^+ \rightarrow HC^{\bullet}O + R_2NH \quad (10)$$

The formyl radical is also observed for DEF, but it is not observed for DMAc-h_9 (Figure 1b). For the latter, the prevalent EPR signal is from $^{\bullet}CH_2N(Me)COMe$ (section 3.5). The EPR spectrum observed for DEF is consistent with the one expected for MeC$^{\bullet}$HN(Et)CHO (section 3.4). Thus, the oxidation of amides involves exclusively (or almost exclusively) the loss of the H_α atom from the corresponding radical cation.

3.3. Radiolysis of *N,N′*-Dimethylformamide. Radiolysis of frozen DMF yields EPR spectra that are different form those observed either in UV photolysis or photooxidation on TiO_2. In Figure 2, we superimposed the EPR spectra obtained in radiolysis of neat DMF-h_7 and DMF-d_7 with the EPR spectra from Figure 1. The triplet of lines from radical **2**-h_6 is present for the radiolyzed sample, but there is an additional contribution from another radical. Assuming that only radical **2**-h_6 contributes to the outer lines of the triplet, we subtracted the normalized EPR spectra to obtain the difference trace shown at the bottom of Figure 2. This trace corresponds to a poorly resolved singlet with a *g*-factor that is greater than radical **2**. This radical (referred to as radical **X**) persists at higher temperature (Figure S10, Supporting Information), while other radicals decay. By superimposing EPR spectra obtained in UV photolysis and 3 MeV radiolysis of neat DMF-h_7 (Figure 3) and DMF-^{15}N (Figure S11, Supporting Information), it is observed that radical **5** provides the main contribution to the wings, accounting for 7−8% of the total radical yield by double integration. Superimposed on the resonance lines from radical **5** are the lines of the formyl radical (Figure 3), with approximately the same relative yield, suggesting that both of these radicals are generated through the scission of the C−N bond in an excited state(s) of the DMF. Closer scrutiny of the EPR spectrum for irradiated DMF-d_7 (Figure 2) reveals the low-field line from DC$^{\bullet}$O superimposed on a weak low-field component of **3**-d_6 (section 3.2). The radiolysis yield of radical **3** relative to radical

dx.doi.org/10.1021/jp2115687 | J. Phys. Chem. A 2012, 116, 1746−1757

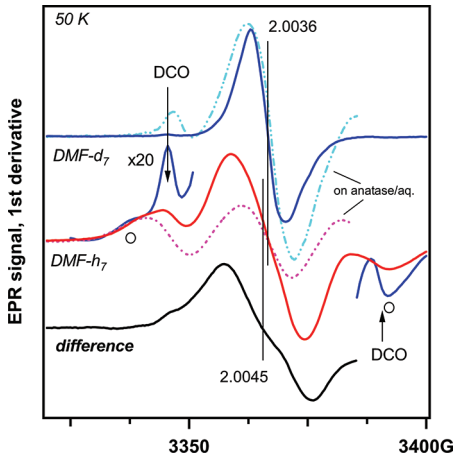

Figure 2. Comparison between the spectra for DMF-h_7 and DMF-d_7 obtained by 3 MeV electron radiolysis of frozen neat liquids (solid lines) and 355 nm photolysis of aqueous TiO_2 nanoparticle solutions (dashed lines). The difference trace for the DMF-d_7 isotopomer is given at the bottom. The open circles indicate $M_z(^{14}N) = \pm 1$ lines from radical **3**-d_7. The arrows indicate the $M_z(D) = \pm 1$ lines from the DC•O radical. The vertical lines indicate the centroids (with the *g*-factor of radical **X** given in the plot).

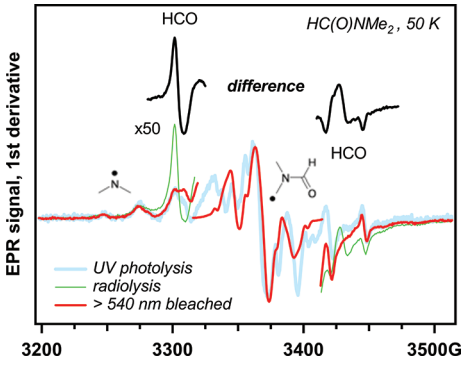

Figure 3. The EPR spectrum of DMF-h_7 irradiated by 3 MeV electrons superimposed on the spectrum of a UV-photolyzed sample. The nonet is from radical **5**-h_7. The doublet is from the formyl radical.

2 is even smaller than this yield in the photooxidation of DMF on anatase.

When the sample irradiated by 3 MeV electrons is subsequently illuminated by red light (670–900 nm, Figure S12, Supporting Information) or yellow light (540–900 nm, Figures 3 and 4), the EPR spectra undergo a dramatic transformation: while radical **5** persists, the HC•O radical and radical **X** disappear. This selective removal allows isolation of the spectral contribution of the formyl radical shown in Figure 3. In Figure 4, we compare (i) the EPR spectra obtained before and after photobleaching of irradiated DMF-h_7 and (ii) the EPR spectrum of radical **2**-h_6 on TiO_2. It is seen that the residual EPR signal is from radical **2** and, by extension, the difference trace must be from radical **X**. The EPR spectrum of radical **X** is revealed to be an asymmetric singlet line. Such an anisotropic ***g***-tensor is unprecedented for cavity-type trapped electrons.

Figure 5a demonstrates the result of a similar treatment for DMF-^{15}N. The EPR spectrum indicated the presence of radical **5**-^{15}N (which is not bleached by light) and the decay of the EPR lines from the HC•O radical and radical **X**. In Figure 5b, we plotted together the difference traces (obtained in the same

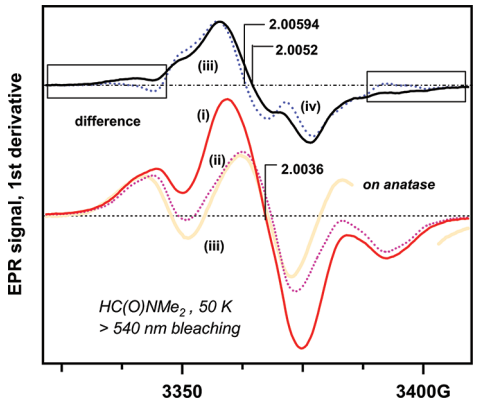

Figure 4. The effect of photobleaching on the central part of the EPR spectrum shown in Figure 3. Trace i is obtained immediately after radiolysis, and trace ii is obtained after bleaching the irradiated sample with yellow light (540–900 nm) for 30 min. The same EPR spectrum is obtained by photobleaching with 670–900 nm light; see Figure S12 in the Supporting Information. For comparison, the trace from DMF-h_7 oxidized on TiO_2 (from Figure 2) is shown. Traces iii and iv are the difference traces obtained for microwave powers of 2 and 0.02 mW, respectively. To produce these difference traces, trace ii was scaled before subtraction to minimize the residual signal in the wings (indicated with rectangles).

manner as the trace shown in Figure 4) for the h_7, ^{15}N, and d_6 isotopomers of DMF. All of these traces are similar (differing only in line width), suggesting that the hfcc's for the ^{14}N and methyl protons in radical **X** are negligibly small.

To obtain further insight into the structure of radical **X**, we performed the same photobleaching experiment with DMF-^{13}CO (Figures 6a and S13, Supporting Information). Since radical **3**-^{13}CO has a large isotropic hfcc on carbonyl ^{13}C (Table S3 and Figure S1, Supporting Information), the corresponding EPR spectrum does not overlap with the central triplet; besides, the yield of radical **3** is very low, and so is the yield of the formyl radical and radical **5**. Thus, the central feature is composed of overlapping lines from the ^{13}CO isotopomers of radical **2** and **X**. This is seen in Figure 6a, as the residual EPR spectrum obtained after photobleaching is identical to the one observed for DMF-h_7 and radical **2**-^{13}CO on TiO_2 (as the hyperfine coupling to carbonyl ^{13}C in radical **2** is negligible, see Table S3 and Figure S1(b), Supporting Information). Thus, the difference trace shown in Figure 6b represents the EPR spectrum of the ^{13}C-carbonyl isotopomer of radical **X**. It is seen from Figure 6b that this EPR spectrum is quite different from the EPR spectra shown in Figure 5b, *indicating a large hfcc on ^{13}C in radical X*. In Figure 6b, we fit the difference traces for DMF-h_7 and DMF-^{13}CO assuming the same anisotropic ***g***-tensor for both isotopomers and a coaxial hfcc tensor for the ^{13}C-labeled isotopomer (see Table 1). This simulation gave highly anisotropic ***g***- and ***A***-tensors for carbonyl ^{13}C with $a(^{13}C) \approx 53.4$ G. *This large isotropic hfcc on ^{13}C excludes solvated/trapped electron as radical X; the latter can only be a carbon-centered species.*

Photobleaching is not the only way to isolate the EPR spectrum of radical **X**, as radical **X** decays while radical **2** persists when the sample is warmed to 100 K, as shown in Figure S14 (Supporting Information). We stress that the high yield of radical **X** (which is comparable to that of radical **2**, as suggested by double integration of the first-derivative EPR spectra) suggests that this radical *is generated via the electron-reduction*

dx.doi.org/10.1021/jp2115687 | J. Phys. Chem. A 2012, 116, 1746–1757

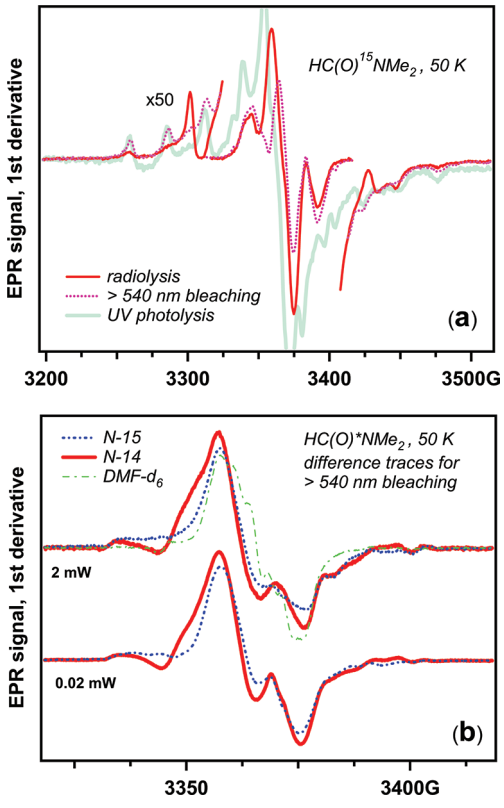

Figure 5. (a) The same as Figure 3, for irradiated frozen DMF-^{15}N; the dotted line is for the sample bleached by yellow light. For comparison, the EPR spectrum (mainly) of radical **5**-^{15}N from UV-photolyzed DMF-^{15}N is superimposed on the EPR spectrum from the radiolyzed sample. (b) Difference traces for DMF-h_7 (solid lines), DMF-^{15}N (dashed lines), and DMF-d_6 (dash-dot lines) obtained in the same fashion as traces iii and iv in Figure 4. The EPR spectrum radical **X** does not change with $^{14}N/^{15}N$ and H/D substitutions in the amide and methyl groups.

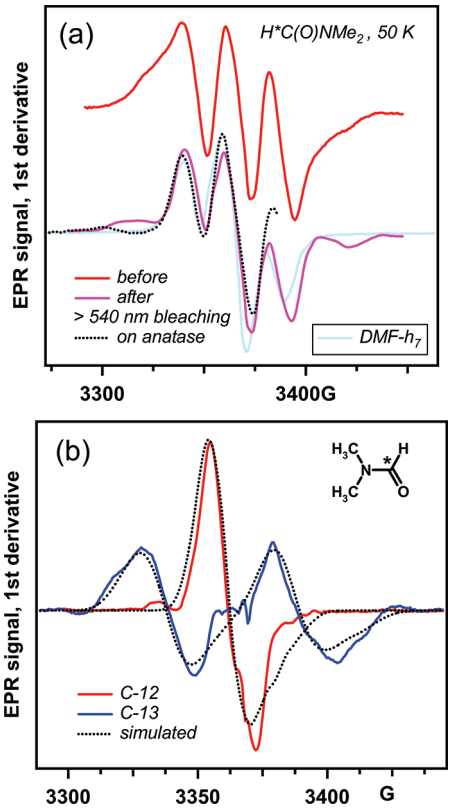

Figure 6. (a) EPR spectra of radiolyzed DMF-^{13}CO before (solid line, to the top) and after (dashed line, to the bottom) photobleaching with yellow light. For comparison, the EPR spectra from DMF-h_7 and DMF-^{13}CO oxidized on TiO_2 are superimposed on the latter trace. It is seen that the main contribution is from radical **2**. (b) Solid lines are the difference traces for DMF-h_7 and DMF-^{13}CO obtained in the same fashion as the difference traces shown in Figures 3 and 5b. The dotted lines are simulated spectra obtained using the magnetic parameters given in Table 1.

pathway. Indeed, for every "hole" yielding radical **2**, there should be a radical derived from the "electron" to maintain charge balance.

As was observed in the Introduction, for frozen formamide[17] and HMPA,[18b] the "electron"-derived radicals observed by EPR are the products of dissociative electron attachment or fragmentation/isomerization reactions (e.g., reactions 7−9). Do such reactions occur in the irradiated DMF?

The experiments using deuterated DMF do suggest this possibility. The need to use such isotopomers stems from the fact that the resonance lines of byproduct radicals are masked by more abundant primary radicals; only when the EPR spectra of these major radicals narrow down due to the H/D substitution (section 2), the EPR features of these minority radicals become apparent. This is illustrated in Figures 7a and S15 (Supporting Information) that exhibit EPR spectra from irradiated DMF-d_7. As expected, this EPR spectrum exhibits a collapsed singlet line from radical **2**-d_6 (for which the hfcc structure on the methyl deuterium becomes apparent in the second-derivative EPR spectrum in Figure 7b) and also radical **X** and the outer lines of a triplet from the DC$^{\bullet}$O radical (Figure 7a and b). The nonet from radical **5**-h_6 transforms into a broad, featureless triplet assigned to **5**-d_6 (cf. Figures S4 and S6(b), Supporting Information), whose lines can be discerned in the EPR spectrum of the photobleached sample (as radical **5** is not photobleached, see Figures 3 and 5). In addition to these

Table 1. Optimized Simulation Parameters for Radicals Observed at 50 K

attribution	$(\delta g_{xx}, \delta g_{yy}, \delta g_{zz})^a$	nuc.	(B_{aa}, B_{bb}, B_{cc}), G	a,[b] G
X, $Me_2N^{13}C^{\bullet}O^-$	(87, 66, −44)	^{13}C	(−15.4, 5.9, 9.5)	53.4
$(CD_3)_2{}^{14}N^{13}C^{\bullet}O$	23[c]	^{14}N	(−2, 6, 8)	22.5
		^{13}C	(−9.7, 17.7, 27.4)	228.7
Y, $Me^{14}N{=}{}^{13}C^{\bullet}OH$	33[c]	^{14}N	(−23.3, −3.3, 26.7)	66.3
		^{13}C	(−10, 0, 10)	55.0

[a] $\delta g = (g - 2) \times 10^4$. [b] Isotropic hfcc. [c] Isotropic g-tensor.

radicals, there are three groups of resonance lines indicated in Figure 7a; all of these radicals can be photobleached.

The doublet of quartets indicated with filled circles is the weakest feature; the relative weight of this EPR signal is comparable to the one expected for ^{13}C satellites of the major radicals in the irradiated DMF. Given the large separation between the quartets, the hfcc for this carbon-13 is ∼230 G, and the interval between the four components is ∼23 G. The same doublet of quartets is observed in irradiated DMF-d_6, as shown in Figure S16(a) (Supporting Information). As argued in section 4.1, this EPR spectrum corresponds to $(CD_3)_2{}^{14}N\,{}^{13}C^{\bullet}O$. The presence of the main isotopomer, $(CD_3)_2{}^{14}N^{12}C^{\bullet}O$, is seen from the lines circled in Figure S16(b)

dx.doi.org/10.1021/jp2115687 | J. Phys. Chem. A 2012, 116, 1746−1757

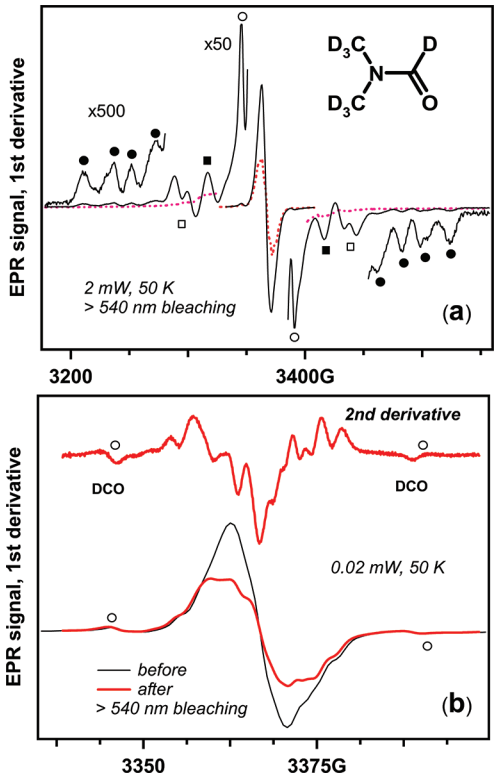

Figure 7. (a) EPR spectra for irradiated DMF-d_7 (solid lines) and the same irradiated sample after photobleaching with yellow light (dashed lines). The resonance lines from the DC•O radical are indicated with open circles; other groups of lines are labeled as in Figure 8. (b) The central line from panel a before (thin line, shown below) and after photobleaching (bold line, shown below) and the second-derivative EPR spectrum of the residual signal (shown to the top). The lines from the DC•O radicals are indicated by open circles.

(Supporting Information) for DMF-d_6, and we remind that this isotopomer of DMF can only yield HC•O radicals that do not produce such lines (which are easy to confuse with the resonance lines of DC•O, see Figure S17(a), Supporting Information).

In contrast, the resonance lines marked with the squares in Figure 7a have no analogues in the other EPR spectra. The composite character of these features is revealed by changing microwave power (Figure S15, Supporting Information) and through different thermal evolution (Figure S17(b), Supporting Information) of the two groups of EPR signals. The group of two doublets indicated with open squares in Figure 7b decays at 100 K, whereas the lines indicated with filled squares persist to 150 K. The former group (attributed to radical **Y**) is also observed in DMF-d_6 (Figure S16(a), Supporting Information), albeit the features of this radical are obstructed by the HC•O radical. The features of radical **Y** are observed in DMF-d_1, suggesting that the hfcc's for the methyl or formyl protons in radical **Y** are small. This means that the large hfcc in this radical lies on the ^{14}N nucleus. Similar features (but more widely spaced) are also observed for DMF-^{13}CO (Figures 8 and S13, Supporting Information). Comparison with the EPR spectrum of radical **5**-h_6 (obtained by UV photolysis of either DMF-h_7 or DMF-^{13}CO) indicates that these features do not originate from radical **5**, nor do these features correspond to the HC•O and $(CH_3)_2{}^{14}N{}^{13}C$•O radicals. Furthermore, both radical **Y** and these lines can be bleached by yellow light (Figure 7) but not

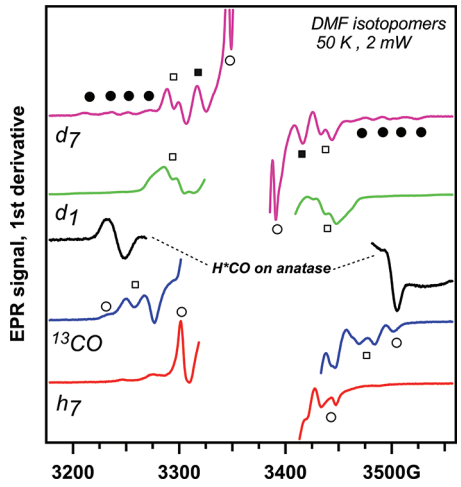

Figure 8. Comparison of the EPR spectra obtained for different isotopomers of DMF, as indicated in the plot. The outer resonance lines for the H^{13}C•O radical are shown for comparison (the lines of the isotopomers of the formyl radical and radical **Y** are indicated by open circles and squares, respectively).

red light (Figure S13, Supporting Information). These observations suggest that these features originate from the ^{13}C-carbonyl isotopomer of radical **Y**; i.e., the unpaired electron in radical **Y** is strongly coupled both to ^{14}N *and* the carbonyl ^{13}C, while it is weakly coupled to the protons. In section 4.1, we suggest that radical **Y** is the *cis*-conformer of MeN═C•OH.

3.4. Radiolysis of *N,N′*-Diethylformamide. Only the perprotio isotopomer of the DEF was studied. Radiolysis of DEF produces the quintet shown in Figure 9a that overlaps with weak signals from the formyl radical. Comparison with the EPR spectrum from Figure 2a reveals the presence of a narrow singlet line analogous to radical **X** in DMF. This line can be bleached by 540−900 nm light (not shown). This EPR spectrum slowly changes after several days of storage at 77 K (Figure 9b), and the residual EPR spectrum does not evolve further upon warming to 100 K (Figure S18, Supporting Information). This EPR spectrum corresponds to the simulated EPR spectrum for the MeC•H(Et)NCHO radical shown in Figure 9b, so it appears that DEF$^{+\bullet}$ preferentially deprotonates from the α-proton site. We conclude that, for DEF and DMF, the observed EPR signal is mainly from radicals **2** and **X**. Since the radiation chemistry of DEF proved to be so close to DMF, it will not be examined further.

3.5. Radiolysis of *N,N′*-Dimethylacetamide. Figure S19 (Supporting Information) shows the EPR spectra obtained for DMAc-h_9, -d_9, and -d_6 photoirradiated on aqueous TiO_2. As seen from this plot, the radical formed by photooxidation of DMAc-h_9 (-d_9) has the same EPR spectrum as radical **2** for DMF-h_7 (-d_7) obtained under the same excitation conditions, with the exception of the presence of the formyl-*h* (-*d*) radical that is absent for DMAc. Furthermore, as the d_9 and d_6 isotopomers of DMAc have identical EPR spectra, it follows that the oxidation occurs exclusively in the Me−N group, which is also the case for DMF (section 3.1).

The EPR spectrum of irradiated DMAc-h_9 (Figure 10a) shows a "skewed" triplet, indicative of the composite nature of this spectrum. Weak resonance lines from radical **5** are observed in the wings, but there is no acetyl radical, which would be the partner of radical **5** had it been formed via the C−N fragmentation of DMAc** (as in UV photolysis, Figure 7).

dx.doi.org/10.1021/jp2115687 | J. Phys. Chem. A 2012, 116, 1746−1757

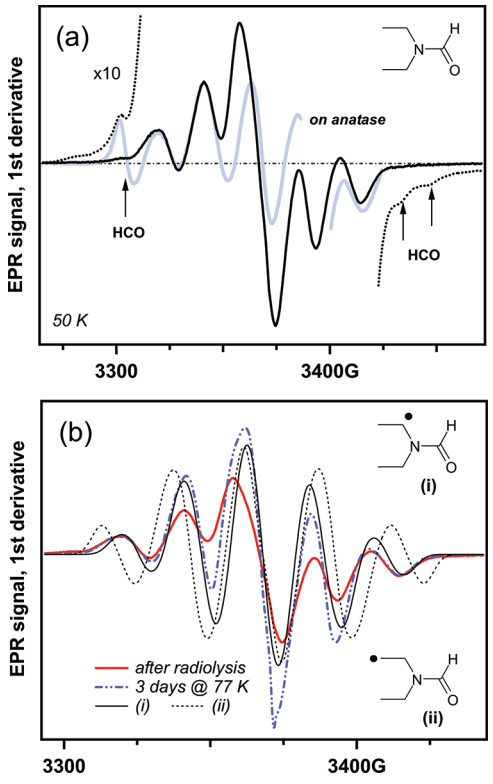

Figure 9. EPR spectra from irradiated DEF at 50 K (solid lines in both panels). (a) A comparison with the EPR spectrum observed for DEF on TiO_2 from Figure 1b. The lines attributed to the formyl radical are indicated with arrows. (b) The EPR spectrum from irradiated DEF before and after storage for three days at 77 K. These spectra are compared to simulated EPR spectra from isomers i and ii of the H atom loss radical of DEF that are shown in the inset.

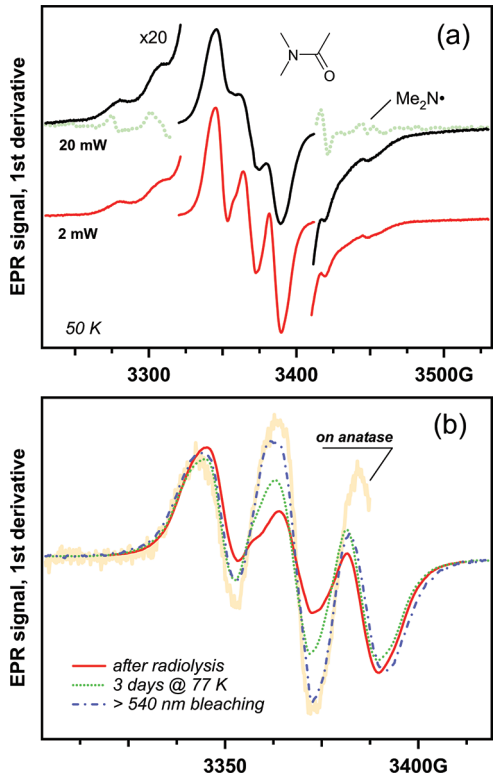

Figure 10. (a) The EPR spectra from 3 MeV electron irradiated DMAc-h_9 obtained immediately after 3 MeV radiolysis. The dashed line is the EPR spectrum from UV-irradiated DMAc-h_9 (originating mainly from radical **5**-h_6). (b) The EPR spectra obtained for the same system but recorded three days after storage at 77 K (dashed line) and after 540−900 nm bleaching (dash-dot line); the solid line corresponds to the spectrum observed immediately after radiolysis. Superimposed is the EPR spectrum of DMAc-h_9 oxidized on TiO_2.

In Figure 10b, we compare the EPR spectra obtained (i) immediately after radiolysis of DMA-h_9, (ii) after three days storage of this sample at 77 K, and (iii) after the irradiated sample that was photobleached with 540−900 nm light. The latter two EPR spectra are very similar to the EPR spectrum obtained by photooxidation of DMAc-h_9 on TiO_2 (Figure 1b). Warming of sample ii to 190 K did not change this EPR spectrum significantly (Figure S20(b), Supporting Information). This triplet is from a methylene radical; however, since the EPR spectra for the $^{\bullet}CH_2(Me)NC(O)Me$ and $Me_2NC(O)C^{\bullet}H_2$ radicals are similar (Figure S21, Supporting Information), the progenitor of this triplet cannot be established with certainty. In Figure S22 (Supporting Information), we subtracted weighed EPR spectra obtained before and after photobleaching (Figure S22(a), Supporting Information) to extract the EPR spectrum of photolytically unstable radical **Z**. This difference trace corresponds to a doublet with $g \approx 2.0045$ and proton hfcc's with $A_x \approx (0-10)$ G, $A_y \approx 0$, and $A_z \approx 48$ G (Figure S22(b), Supporting Information).

The coupled proton in radical **Z** can originate either from the Me−N or Me−C methyl groups. To determine the source, several isotope configurations were examined. As shown in Figure S23 (Supporting Information), radiolysis yields similar EPR spectra for DMAc-d_3 and DMAc-h_9, which suggests that the prevalent contribution in both of these spectra is from radical **2**. This is further demonstrated in Figure S24 (Supporting Information), as photobleaching of both of these samples yields a radical whose EPR spectrum is identical to that of radical **2** observed on TiO_2 (Figure S19, Supporting Information). Since deuteration in the Me−C group does not change the EPR spectrum of the $^{\bullet}CH_2N(CH_3)C(O)CH_3$ radical, the photostable species can only be this radical. Radiolysis of DMAc-d_9 yields an EPR spectrum in which the resonance lines of radicals **2** and **Z** have collapsed to a singlet (Figure S23, Supporting Information). The most telling features are exhibited by the EPR spectrum for DMAc-d_6. The corresponding $^{\bullet}CD_2N(CD_3)C(O)CH_3$ radical has an EPR spectrum corresponding to a singlet line, as shown in Figure S19 (Supporting Information). The EPR spectrum of DMAc-d_6 reveals two side lines indicated with arrows in the plot. The central singlet is more saturable than these side lines, suggesting that the latter belong to another radical. Photobleaching selectively removes these side lines (Figure S24, Supporting Information), revealing the residual singlet line of radical **2**-d_6. Since our results (see above) indicate that an H atom loss in the precursor radical cation occurs *exclusively* from the Me−N group, these side lines can only be from radical **Z**, and the lone coupled proton originates from the Me−C group. This is also suggested by the photobleaching pattern observed for DMAc-d_9 (Figure S24, Supporting Information), as the removed radical has a narrow EPR spectrum, which corresponds to the *d*-isotopomer of radical **Z**.

We conclude that radiolysis of DMAc yields two major radical species, radicals **2** and **Z**, in approximately the same yield. This suggests that radical **Z** is generated via an electron-reduction channel, like radical **X** for DMF and DEF.

dx.doi.org/10.1021/jp2115687 | J. Phys. Chem. A 2012, 116, 1746−1757

4. DISCUSSION

4.1. *N,N′*-Dimethylformamide. The high yield of H atom loss radicals via a site-selective deprotonation of the parent radical cations (sections 3.2 and 3.3) can be anticipated in the view of previous work indicating such reactions for matrix-isolated radical cations.[21,22] Likewise, the occurrence of C−N bond scission leading to the formation of the formyl radical and radical **5**, albeit as a minor process, is expected: such dissociation can occur either through fragmentation in the excited state (section 3.1) or via reactions 3a and 3b involving prethermalized electrons. What is unexpected is the apparent high selectivity of this fragmentation: despite the relatively small difference between the energies of the C−H and C−N bonds for carbonyl and methyl carbons (Table S1, Supporting Information), no radicals **6** and **7** (Scheme 1) were found and only a very low yield of radical **3** was observed. This low yield cannot be explained by the secondary reactions of such radicals, as these can be readily generated in the same matrix photolytically (section 3.1 and ref 23).

The most surprising part of the observed radiation chemistry is the electron (reductive) channel. By analogy to the known chemistry of formamide (reactions 7, 8, and 9), we expected that electron attachment to DMF would yield unstable radical **9** (or its protonated form, radical **8**; see Scheme 1) which eliminates the methoxide anion (or methanol) and yields radical **11**, subsequently rearranging to radical **12**. We have simulated EPR spectra of these radicals in Figure S8 (Supporting Information; the estimated hfcc's are given in Table S3); none of these EPR spectra correspond to the species observed. The chemistry of formamide appears to be unique to this molecule.

Instead, our experiments pointed to radical **X**. This radical is the only paramagnetic species whose yield is comparable to that of radical **2** (which is a product of *oxidative* reactions). This parity implies that this species is generated via *electron* reactions. Since the electron affinity of the solvent is negligible, we expected that the released electrons would react with proton adducts **4** generated via the deprotonation of radical cations. Neutralization of this adduct yields radical **8** or releases mobile, reactive H• atoms; the latter would abstract hydrogens from methyl or formyl groups (yielding radicals **2** and **3**, respectively) or possibly add to the >C═O group. In Figure 11a, we simulated the EPR spectrum of radical **8** using hfcc parameters obtained in our DFT calculations (Table S3, Supporting Information). As expected from the literature data for close analogues of radical **8** (Table S3, Supporting Information), the latter has a large hfcc in the formyl proton, and the EPR spectrum of this radical corresponds to a doublet rather than a singlet. Thus, radical **X** cannot be radical **8**. In section 3.3, we demonstrated that radical **X** has negligible hfcc's in all of the magnetic nuclei except for carbonyl ^{13}C. This identifies this radical as being carbon-centered, excluding previously suggested radical **10**. We emphasize that the unpaired electron is coupled to a single carbonyl carbon, i.e., radical **X** cannot be a cavity electron or dimer/multimer radical anion.

Our DFT calculations indicate only two structures fulfilling these criteria: parent anion radical **9** and $Me_2NC^{\bullet}(OH)_2$ (Figure 10b and Tables S2 and S3, Supporting Information) which is the hydrated form of radical **3**. While our DFT calculations predict comparable ^{13}C tensors for these two radicals (Table 1), such estimates are not very reliable, as the only way to retain an electron on the gas-phase DMF molecule was to provide a tight set of molecular orbitals (so the electron is

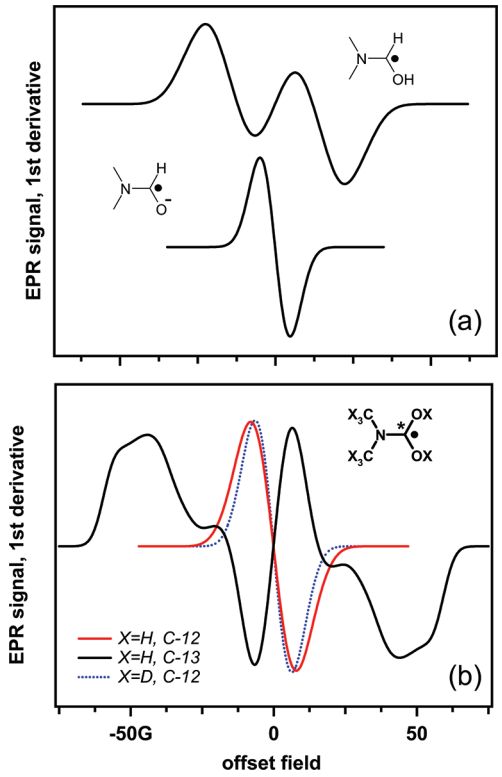

Figure 11. Simulated EPR spectra for (a) radicals **8** and **9** and (b) the isotopomers of $Me_2NC^{\bullet}(OH)_2$. The isotropic *g*-tensor was assumed in these simulations.

forced into a C 2p antibonding orbital), imitating the situation in the condensed phase, where the solvent molecules exclude diffuse orbitals. As the hfcc tensor for ^{13}C depends on the population of this antibonding orbital, such a method cannot yield a reliable estimate. Our arguments in favor of radical **9** are 2-fold. First, it is difficult to see how $Me_2NC^{\bullet}(OH)_2$ could be produced in a solvent containing very little water, especially at low temperature. Second, it is difficult to see how photoexcitation of this radical with visible light can result in its decay (and no concomitant emergence of the $Me_2N^{\bullet}$ radical), as such radicals (i) do not absorb in the visible and (ii) have no obvious photoisomerization or fragmentation pathways. In contrast, electron photodetachment from weakly bound radical **9** readily explains the experimental observations.

On the strength of these arguments, we identify radical **X** with the monomer radical anion of DMF. This radical is unstable photolytically, which is understandable given that this *solvent supported* radical anion is stabilized through the polarization of solvent molecules around the anion (in this sense, this anion is similar to a cavity electron); the electron should be readily photodetached from this anion. A similar situation is known to occur in acetonitrile, where the dimer radical anion is stabilized through interactions with other solvent molecules.[30,31] There are some other examples of such anion stabilization in the literature, e.g., for liquid benzene (see review in ref 6).

What makes this radical chemically stable? Low proton mobility in solid DMF could explain the impeded recombination with the proton adduct, and the high energetic cost of elimination of MeO^-/MeOH could explain the inefficiency of

dx.doi.org/10.1021/jp2115687 | J. Phys. Chem. A 2012, 116, 1746−1757

reaction 8. However, our results point to another possibility: radical anion **9** undergoes methane elimination

$$Me_2NC^{\bullet}HO^{-} \rightarrow MeNC^{\bullet}O^{-} + CH_4 \quad (11)$$

According to our DFT calculations (Table S1, Supporting Information), in the gas phase reaction 11 is exergonic by 0.62 eV. We suggest that the resulting radical $MeN{=}C^{\bullet}O^{-}$ becomes protonated

$$MeNCO^{-\bullet} + H^{+} \rightarrow MeN{=}C^{\bullet}OH \quad (12)$$

and the *cis*-conformer of this protonated radical is radical **Y**. Our search for candidate radicals failed to produce another radical that has negligible hfcc's in the methyl and formyl protons *and* large hfcc's in the ^{14}N and carbonyl ^{13}C nuclei. The need for such hfcc's is suggested by the simulations shown in Figure 12a and the optimum hfcc parameters given in Table 1. These large hfcc's indicate $^{14}N{=}^{13}C$ coupling in the progenitor, and $MeN{=}C^{\bullet}OH$ is the best candidate species exhibiting such features, despite the fact that the hfcc's estimated by DFT are somewhat different from those obtained in EPR simulations.

Another radical of interest is the progenitor of the features shown in Figure 12b which we attributed to the ^{13}C satellites of radical **3**. For gas-phase radical **3**, our DFT calculation yields an isotropic hfcc on ^{13}C that is considerably lower than obtained experimentally (155 G vs 229 G), while this DFT estimate is consistent with the ~150 G value reported for *tert*-BuNHC$^{\bullet}$O and $H_2NC^{\bullet}O$.[43] This discrepancy can be accounted for by matrix effects, namely, by distortions of this radical from planarity. As suggested by the DFT calculations shown in Figure S2(a), such an increase can also occur in radical **3** protonated at the nitrogen atom (Table S3, Supporting Information). This protonation (which, in the gas phase, is 180 meV less favorable than protonation at the oxygen atom in the carbonyl group) results in a relatively small change in the hfcc for ^{14}N but causes a substantial increase in the hfcc for ^{13}C (to ~240 G). Thus, our results could indicate that radical **3** is generated via the isomerization of $\{DMF\}^{+\bullet}$ through a 1,2-shift of the formyl hydrogen (competing with reaction 5) rather than C−H bond scission in {DMF}**

$$\{Me_2NCHO\}^{+\bullet} \rightarrow Me_2HN^{+}C^{\bullet}O \quad (13)$$

4.2. *N,N′*-Dimethylacetamide. Radiolysis of DMF and DEF yields a radical anion whose hyperfine constants broadly agree with our tight-binding DFT calculation; on the other hand, radiolysis of DMAc yields radical **Z** whose EPR spectrum does not agree with our calculations. Unfortunately, the tight binding could misrepresent the orbital structure of a solvent-stabilized anion, and we believe that the discrepancy results from the crudeness of our approach.

Indeed, the EPR spectrum and hfcc parameters for radical **Z** are nearly identical to the radical anion of acetamide-d_2 (D_2NCOMe) observed by Sevilla[36] using electron photodetachment from $Fe(CN)_6^{4-}$ in 8 M NaOD/D_2O. A 30.8 G doublet corresponding to a single coupled methyl proton was observed at 85 K; as the temperature increased to 180 K, this doublet gradually resolved into a 1:3:3:1 quartet for a freely rotating methyl group with $a(^1H)$ = 13.5 G. This transformation is reversed by cooling the sample back to 85 K.[36] For radical **Z**, we observed the 28.9 G doublet shown in Figure 10b. The softness of the DMAc matrix and the obscuring EPR signal from radical **2** made it impossible to observe gradual onset of

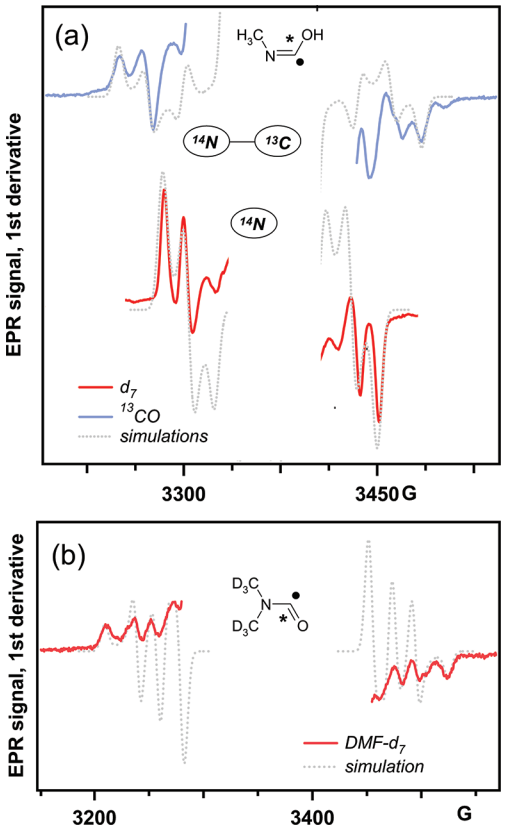

Figure 12. Simulated EPR spectra (dashed lines) for the outer lines in irradiated DMF-d_7 and DMF-^{13}CO (the solid lines are for experimental traces). (a) Simulation of the groups of lines indicated by open squares in Figures 7a and 8 (attributed to isotopomers of radical **Y**) using the magnetic parameters given in Table 1. These lines are attributed to *cis*-$CH_3{}^{14}N{=}^{12,13}C^{\bullet}OH$, as shown in the inset. (b) Simulation of the features indicated with filled circles in Figures 7a and 8, attributed to the $(CD_3)_2N^{13}C^{\bullet}O$ or $(CD_3)_2DN^{+13}C^{\bullet}O$ radical. See Table 1 for simulation parameters.

methyl group rotation in radical **Z**. Suryanarayana and Sevilla[37] suggested that, at low temperature, the Me−C group is locked in a position where the C−H bond (for the single coupled proton) is collinear with the carbonyl C $2p_z$ orbital (in which the carbon is pyramidal). We address the reader to ref 37 for more detail, as we believe that Me−N substitution and matrix replacement do not significantly affect the structure of this radical anion. We suggest that, in frozen DMAc, the trapped electron center is also a solvent-stabilized radical anion.

5. CONCLUDING REMARKS

The inherent difficulty in the studies of electron localization is that there are no firm criteria that allow distinction between solvent-stabilized multimer/monomer anions and "solvated electrons". NMR studies of alkali solutions of ammonia, amines, and HMPA (see refs 16 and 17 for a review) have suggested extensive unpaired electron sharing in the antibonding orbitals of several solvent molecules; to a first approximation, the electron in such liquids can be regarded as a "solvated electron". Amides, due to their structural similarity to these molecules, have been regarded in the same way. Many of these amides, such as *N,N′*-diethylacetamide, *N,N′*-dipropylacetamide, *N,N′*-dimethylpropanamide, tetramethylurea, and tetraethylurea, yield blue solutions when metallic sodium is dissolved in such liquids,[14] just like in ammonia and amines. The optical

dx.doi.org/10.1021/jp2115687 | J. Phys. Chem. A 2012, 116, 1746−1757

and EPR spectra and photobleaching behavior of excess electrons in liquid and solid amides are supportive of the cavity model (see the Introduction), and this model provides a coherent and minimalistic explanation of many of the properties observed. Despite all of these appearances, we have shown that excess electrons in frozen amides are solvent-stabilized monomer radical anions rather than the cavity electrons.

Since the absorption spectra for irradiated solid[23] and liquid[14,29,34] amides are similar, it is likely that the mode of electron localization in solid and liquid amides is also similar. While this conclusion is plausible, it is not necessarily correct, as suggested by the example of acetonitrile, for which crystalline α-acetonitrile supports exclusively a C−C bound dimer radical anion,[30] whereas, in the liquid, cavity electrons (or the multimer radical anion, depending on one's intellectual preference)[44] and this dimer anion coexist in equilibrium.[31−33,44] These two species have quite different optical spectra and charge mobility, and they interconvert sufficiently slowly to distinguish them spectroscopically and chemically.[31] In other liquids, such species may interconvert too rapidly or have spectra and reactivity that are too similar to clearly distinguish them. No experimental methods currently exist to recognize or characterize such electronic states, whereas organic molecules typically possess 2p orbitals that are accessible to the electron, if only fleetingly. The appearances could be even more deceptive.

Our study emphasizes the need to develop first-principle models for electron localization in organic liquids. While using tight binding sets for isolated molecules provided more or less a correct picture in some cases (DMF), it failed in other cases (DMAc), suggesting that the solvent should be treated explicitly. Even in the situation when electron localization occurs preferentially on a single solvent molecule, the phenomena that give rise to "solvated electrons" are still at work, and the need for accurate modeling remains pressing.

■ ASSOCIATED CONTENT

Supporting Information

A PDF file containing a list of abbreviations and reactions, Tables S1−S3, and Figures S1−S24 with captions, including the experimental and simulated EPR spectra. This material is available free of charge via the Internet at http://pubs.acs.org.

■ AUTHOR INFORMATION

Corresponding Author

*Phone: (630) 252-9516. E-mail: shkrob@anl.gov.

Notes

The authors declare no competing financial interest.

■ ACKNOWLEDGMENTS

I.A.S. thanks R. Lowers, D. Quigley, S. Chemerisov, and J. Muntean for technical support. The work at Argonne was supported by the US-DOE Office of Science, Division of Chemical Sciences, Geosciences and Biosciences under Contract No. DE-AC-02-06CH11357. Programmatic support via a DOE SISGR grant "An Integrated Basic Research Program for Advanced Nuclear Energy Separations Systems Based on Ionic Liquids" is gratefully acknowledged.

■ REFERENCES

(1) Berthon, L.; Chabronnel, M.-C. In *Ion Exchange and Solvent Extraction, A Series of Advances*, Vol. *19*; Moyer, B. A., Ed.; CRC Press: Boca Raton, FL, 2010; pp 429−513; diglycolamide and monoamide based metal ion separations, such as the novel AIST process involving normal and branched R_2NCOR monoamides, are also examined by: Ansari, S. A.; Pathak, P.; Mohapatra, P. K.; Manchanda, V. K. *Chem. Rev.* **2012**, DOI: 10.1021/cr200002f.

(2) Wishart, J. F. *J. Phys. Chem. Lett.* **2010**, *1*, 3225−3231. Wishart, J. F.; Shkrob, I. A. In *Ionic Liquids: From Knowledge to Application*; Rogers, R. D., Plechkova, N. V., Seddon, K. R., Eds.; American Chemical Society: Washinton, DC, 2009; pp 119−134.

(3) Ben-Amotz, D. *J. Phys. Chem. Lett.* **2011**, *2*, 1216−1222 and references therein. Jordan, K. D.; Johnson, M. A. *Science* **2010**, *329*, 42−43.

(4) Larsen, R. E.; Glover, W. J.; Schwartz, B. J. *Science* **2010**, *329*, 65−69. Turi, L.; Madarasz, A. *Science* **2011**, *331*, 1387. Jacobson, L. D.; Herbert, J. M. *Science* **2011**, *331*, 1387. Larsen, R. E.; Glover, W. J.; Schwartz, B. J. *Science* **2011**, *331*, 1387. See also: Abel, B.; Buck, U.; Sobolewski, A. L.; Domcke, W. *Phys. Chem. Chem. Phys.* **2012**, *14*, 22−34.

(5) Herbert, J. M.; Jacobson, L. D. *J. Phys. Chem. A* **2011**, *115*, 14470−14483 and a discussion therein.

(6) Shkrob, I. A.; Sauer, M. C., Jr. In *Charged Particle and Photon Interactions with Matter. Chemical, Physicochemical, and Biological Consequences with Applications*; Hatano, Y., Mozumder, A., Eds.; Marcel Dekker: New York, 2004; Ch. 11, pp 301−331.

(7) Shkrob, I. A.; Glover, W. J.; Larsen, R. E.; Schwartz, B. J. *J. Phys. Chem. A* **2007**, *111*, 5232−5243. Shkrob, I. A. *J. Phys. Chem. A* **2007**, *111*, 5223−5231.

(8) Hare, P. M.; Price, E. A.; Stanisky, C. M.; Janik, I.; Bartels, D. M. *J. Phys. Chem. A* **2010**, *114*, 1766−1775. Marsalek, O.; Uhlig, F.; VandeVondele, J.; Jungwirth, P. *Acc. Chem. Res.* **2012**, *45*, 23−32.

(9) Boero, M.; Parrinello, M.; Terakura, K.; Ikeshoji, T.; Liew, C. C. *Phys. Rev. Lett.* **2003**, *90*, 226403 and references therein.

(10) Hart, E. J.; Anbar, M. *The Hydrated Electron*; Wiley-Interscience: New York, 1970.

(11) Shkrob, I. A. In *Recent Trends in Radiation Chemistry*; Wishart, J. F., Rao, B. S. M., Eds.; Word Scientific: Singapore, 2010; pp 59−96.

(12) Holton, D. M.; Edwards, P. P.; Johnson, D. C.; Page, C. J.; McFarlane, W.; Wood, B. *J. Am. Chem. Soc.* **1985**, *107*, 6499−6504.

(13) Edwards, P. P. *J. Solution Chem.* **1985**, *14*, 187−208 and references therein.

(14) Young, C. A.; Dewald, R. R. *J. Chem. Soc., Chem. Commun.* **1977**, 188−189. We note that while the property of supporting chemically stable solvated electrons via Na^- dissociation to (Na^0,e_{solv}^-) pertains to some amide liquids, DMF, DEF, and DMAc are known to react with Na^-; see: Young, C. A.; Dewald, R. R. *J. Am. Chem. Soc.* **1979**, *101*, 2884−2888.

(15) Langan, J. R.; Liu, K. J.; Salmon, J. A.; Edwards, P. P.; Ellaboudy, A.; Holton, D. M. *Proc. R. Soc. London, Ser. A* **1989**, *421*, 169−178.

(16) Shkrob, I. A. *J. Phys. Chem. A* **2006**, *110*, 3967−3976. See also: Meyer, A.; van Gastel, M. *J. Phys. Chem. A* **2011**, *115*, 1939−1945. Chiesa, M.; Giamello, E.; Van Doorslaer, S. *J. Am. Chem. Soc.* **2009**, *131*, 12664−12670.

(17) Zurek, E.; Edward, P. P.; Hoffmann, R. *Angew. Chem., Int. Ed.* **2009**, *48*, 8198−8232 and references therein.

(18) (a) Chen, H.-L. J.; Bersohn, M. *J. Am. Chem. Soc.* **1966**, *88*, 2663−2665. Dodin, G; Dubois, J. E. *J. Phys. Chem.* **1973**, *77*, 2483−2487. (b) Rao, K. V. S.; Symons, M. C. R. *J. Chem. Soc., Faraday Trans. 2* **1972**, *68*, 2081−2086.

(19) Shkrob, I. A.; Marin, T. W.; Chemerisov, S. D.; Wishart, J. F. *J. Phys. Chem. B* **2011**, *115*, 10927−10942.

(20) Colebourne, N.; Collinson, E.; Dainton, F. S. *Trans. Faraday Soc.* **1963**, *59*, 886−894.

(21) Mel'nikov, M. Ya.; Belevskii, V. N.; Belopushkin, S. I.; Mel'nikova, O. L. *Russ. Chem. Bull.* **1997**, *46*, 1245−1247.

(22) Qin, X.-Z.; Pentecost, T. C.; Wang, J. T.; Williams, F. *J. Chem. Soc., Chem. Commun.* **1987**, 450−453. Eastland, G. W.; Rao, D. N. R.; Symons, M. C. R. *J. Chem. Soc., Faraday Trans. 1* **1986**, *82*, 2833−2842.

(23) Pukhal'skaya, G. V.; Kotov, A. G.; Pshezhetskii, S. Ya. *High Energy Chem.* **1969**, *3*, 340−345.

(24) Forde, N. R.; Butler, L. J.; Abrash, S. A. *J. Chem. Phys.* **1999**, *110*, 8954−8968.
(25) Dusaucy, A.-C.; De Doncker, J.; Couillard, C.; De Laet, M.; Tilquin, B. *J. Chem. Soc., Faraday Trans. 1* **1987**, *83*, 125−133.
(26) Trofimov, V. I.; Chkheidze, I. I. *High Energy Chem.* **1967**, *1*, 324−335.
(27) Symons, M. C. R. *Tetrahedron* **1973**, *29*, 615−619.
(28) Desfrançois, C.; Périquet, V.; Carles, S.; Schermann, J. P.; Adamowicz, L. *Chem. Phys.* **1998**, *239*, 475−483.
(29) Hayashi, N.; Hayon, E.; Ibata, T.; Lichtin, N. N.; Matsumoto, A. *J. Phys. Chem.* **1971**, *75*, 2257−2272.
(30) Shkrob, I. A.; Takeda, K.; Williams, F. *J. Phys. Chem. A* **2002**, *106*, 9132−9144.
(31) Shkrob, I. A.; Sauer, M. C. Jr. *J. Phys. Chem. A* **2002**, *106*, 9120−9131. Xia, C.; Peon, J.; Kohler, B. *J. Chem. Phys.* **2002**, *117*, 8855 (12 pages).
(32) Mitsui, M.; Ando, N.; Kokubo, S.; Nakajima, A.; Kaya, K. *Phys. Rev. Lett.* **2003**, *91*, 153002 (4 pages).
(33) Ehrler, O. T.; Neumark, D. M. *Acc. Chem. Res.* **2009**, *42*, 769−777. Ehrler, O. T.; Griffin, G. B.; Young, R. M.; Neumark, D. M. *J. Phys. Chem. B* **2009**, *113*, 4031−4037. Young, R. A.; Griffin, G. B.; Kammrath, A.; Ehrler, O. T.; Neumark, D. M. *Chem. Phys. Lett.* **2010**, *485*, 59−63.
(34) Tran-Thi, T. H.; Koulkes-Pujo, A. M. *J. Phys. Chem.* **1983**, *87*, 1166−1169.
(35) Bedard-Hearn, M. J.; Larsen, R. E.; Schwartz, B. J. *J. Chem. Phys.* **2006**, *125*, 194509 (8 pages). Bedard-Hearn, M. J.; Larsen, R. E.; Schwartz, B. J. *J. Chem. Phys.* **2004**, *122*, 134506 (11 pages).
(36) Sevilla, M. D. *J. Phys. Chem.* **1970**, *64*, 669−672.
(37) Suryanarayana, D.; Sevilla, M. D. *J. Phys. Chem.* **1990**, *84*, 3045−3049.
(38) Shkrob, I. A.; Sauer, M. C. Jr. *J. Phys. Chem. A* **2006**, *110*, 8126−8136. Shkrob, I. A.; Sauer, M. C. Jr. *J. Phys. Chem. A* **2005**, *109*, 5754−5769. Shkrob, I. A.; Sauer, M. C. Jr. *J. Phys. Chem. B* **2001**, *105*, 7027−7032.
(39) Shkrob, I. A.; Marin, T. W.; Adhikary, A.; Sevilla, M. D. *J. Phys. Chem. C* **2011**, *115*, 3393−3403.
(40) Becke, A. D. *Phys. Rev. A* **1988**, *38*, 3098. Lee, C.; Yang, W.; Parr, R. G. *Phys. Rev. B* **1988**, *37*, 785.
(41) Hariharan, P. C.; Pople, J. A. *Theor. Chim. Acta* **1973**, *28*, 213.
(42) Frisch, M. J.; Trucks, G. W.; Schlegel, H. B.; Scuseria, G. E.; Robb, M. A.; Cheeseman, J. R.; Zakrzewski, V. G.; Montgomery, J. A., Jr.; Stratmann, R. E.; Burant, J. C., et al. *Gaussian 98*, rev. A.1; Gaussian, Inc.: Pittsburgh, PA, 1998.
(43) Landolt-Bornstein, New Series, *Magnetic Properties of Free Radicals*; Fischer, H., Ed.; Springer-Verlag: Berlin, 1987.
(44) Takayanagi, T. *Chem. Phys.* **2004**, *302*, 85−93. Takayanagi, T. *J. Chem. Phys.* **2005**, *122*, 244307 (8 pages). Timerghazin, Q. K.; Peslherbe, G. H. *J. Phys. Chem. B* **2008**, *112*, 520−528. Azar, J.; Kurlancheek, A. J.; Head-Gordon, M. *Phys. Chem. Chem. Phys.* **2011**, *13*, 9147−9154.